Behavior of sulfate ions during biogenic scorodite crystallization from dilute As(III)-bearing acidic waters

Tanaka, Masahito
Department of Earth Resource Engineering, Faculty of Engineering, Kyushu University

Sasaki, Keiko
Department of Earth Resource Engineering, Faculty of Engineering, Kyushu University

Okibe, Naoko
Department of Earth Resources Engineering, Faculty of Engineering, Kyushu University

出版情報：Hydrometallurgy. 180, pp.144-152, 2018-09. Elsevier
バージョン：
権利関係：

Behavior of sulfate ions during biogenic scorodite crystallization from dilute As(III)-bearing acidic waters

Masahito TANAKA, Keiko SASAKI, Naoko OKIBE

PII: S0304-386X(18)30079-3
DOI: doi:10.1016/j.hydromet.2018.07.018
Reference: HYDROM 4873

To appear in: *Hydrometallurgy*

Received date: 23 February 2018
Revised date: 28 June 2018
Accepted date: 19 July 2018

Please cite this article as: Masahito TANAKA, Keiko SASAKI, Naoko OKIBE , Behavior of sulfate ions during biogenic scorodite crystallization from dilute As(III)-bearing acidic waters. Hydrom (2018), doi:10.1016/j.hydromet.2018.07.018

Hydrometallurgy (IBS Special Issue)

Behavior of sulfate ions during biogenic scorodite crystallization from dilute As(III)-bearing acidic waters

Masahito TANAKA, Keiko SASAKI, Naoko OKIBE*

Department of Earth Resources Engineering, Faculty of Engineering, Kyushu University, 744 Motooka, Nishi-ku, Fukuoka 819-0395, Japan

*Corresponding author.

Tel. and Fax: + 81 92 802 3312

E-mail address: okibe@mine.kyushu-u.ac.jp (Naoko OKIBE)

Keywords: arsenic, biogenic scorodite, sulfate ion, phase transformation

Abstract

This study revealed the importance of SO_4^{2-} ions during biogenic scorodite crystallization via a two-stage As-removal process, using a combination of liquid and solid analyses (chemical digestion, FT-IR, SEM, TG-DTA, particle distribution). The first-stage As-removal was induced by microbial oxidation of Fe^{2+} and As(III), precipitating SO_4^{2-}-bearing amorphous precursors composed of basic ferric sulfate ($MFe_x(SO_4)_y(OH)_z$) and ferric arsenate ($FeAsO_4 \cdot (2+n)H_2O$). This was followed by an induction period (a period of constant concentration), where dissolution-recrystallization of unstable amorphous precursors proceeded: Re-dissolved metal ions became locally concentrated on the surface of precursors, which gave the driving force for the second-stage As-removal as secondary layers of crystalline biogenic scorodite ($Fe(AsO_4)_{0.94}(SO_4)_{0.08} \cdot 1.69H_2O$) out of even more dilute and seeded solution. This phase transformation process was also accompanied by continuous dehydration. This two-stage As-removal via SO_4^{2-}-mediated phase transformation was shown to be key to promote biogenic scorodite formation with greater final As-removal from dilute As(III)-bearing solutions.

1. Introduction

Contamination of arsenic (As) in metal refinery wastewaters is a growing problem especially owing to an increasing demand to process low-grade, even As-bearing copper sulfides such as enargite (Cu_3AsS_4) and tennantite ($Cu_{12}As_4S_{13}$). Highly toxic As(III) is often the form of the As contaminant in such wastewaters and its appropriate immobilization is essential. Strict regulatory limits have been set for landfill of As compounds: e.g. USA, 5 mg/l As (Toxicity characteristic leaching procedure, TCLP; EPA 1992); Japan, 0.3 mg/l As (Environment Agency notification No.46)).

Scorodite ($FeAsO_4{\cdot}2H_2O$) is considered as one of the most ideal As-disposal forms due to its thermodynamic stability ($K_{sp} = 10^{-25.8}$), high density and low iron demand (Fe/As ≈ 1) (Langmuir et al., 2006; Riveros et al., 2001). Scorodite synthesis tends to become increasingly challenging at more dilute As(III) solutions. However, attempts to crystallize biogenic scorodite directly from dilute 3.3-20 mM As(III) solutions at 70°C, solely via microbiological oxidation of Fe^{2+} and As(III), have been successful by using the extremely acidophilic, thermophilic archaeon *Acidianus* (*Ac.*) *brierleyi* (Okibe et al., 2014, 2017; Tanaka and Okibe, 2018). These low As(III) concentrations are generally below the ideal concentration range for chemical scorodite syntheses: i.e., previous hydrothermal and atmospheric chemical scorodite studies targeted concentrated pre-oxidized As(V) solutions of 75–667 mM (Dutrizac and Jambor, 1988; Monhemius and Swash, 1999; Gomez et al., 2011; Filippou and Demopoulos, 1997; Fujita et al., 2008a, 2008b, 2009; Singhania et al., 2005, 2006). The advantage in employing microbes in scorodite formation from dilute As(III) solutions lies in the microbial cells capable of locally accumulating the metal species within the EPS (Extracellular Polymeric Substances) region, thus facilitating the initial crystal

nucleation within this reaction compartment (Okibe et al., 2013, 2014). Scorodite seed-feeding can further promote this phenomenon by providing the surface for cell colonization (Okibe et al., 2017) and for electrostatic As(V) absorption (Okibe, unpublished data). Biogenic scorodite possesses characteristic spherical morphology compared to chemically synthesized orthorhombic crystals (Okibe et al., 2014; Tanaka and Okibe, 2018) with fewer (< 2) hydration H_2O molecules (Tanaka and Okibe, 2018), while its stability was shown to be generally comparable to those chemically synthesized (Tanaka and Okibe, 2018).

In the biogenic scorodite method using *Ac. brierleyi*, optimizing conditions such as initial $[Fe^{2+}]/[As(III)]$ molar ratio, initial pH and seed feeding showed a significant effect on improvement of final As-removal and product stability (Tanaka and Okibe, 2018). Biogenic scorodite precipitated immediately as a single-stage process at the initial pH 1.2. Although increasing the initial pH to 1.5 led to a typical two-stage As-removal (rapid formation of brown amorphous precursors was followed by crystallization of whitish biogenic scorodite particles), this eventually allowed a greater final As-removal (Tanaka and Okibe, 2018). It was therefore considered that this two-stage As-removal holds the key to effective biogenic scorodite crystallization from dilute As(III) solutions.

Meanwhile, metal refinery wastewaters typically contain sulfate (SO_4^{2-}) ions and the effects of SO_4^{2-} on chemical scorodite syntheses have been reported: e.g., Demopoulos et al. (1995) reported an inhibitory effect of SO_4^{2-} (100 mM) in scorodite yield in 2 g/L (27 mM) As(V)-Fe^{3+}-HCl solution in atmospheric synthesis. Substitution of SO_4^{2-} with AsO_4^{3-} in scorodite was observed using 25 g/L (334 mM) As(V)-Fe^{3+}-HNO_3 medium by addition of ~2 M Li_2SO_4 in hydrothermal synthesis (Dutrizac

and Jambor, 1988). Incorporation of SO_4^{2-} in scorodite was suggested by excess addition of SO_4^{2-} (1-2 M) in 10 g/L (133 mM) As(V)-Fe^{3+}-H_2SO_4 solution in atmospheric synthesis (Singhania et al., 2006).

Since biogenic scorodite formation is regularly conducted with excess SO_4^{2-} (65 mM at pH 1.5) relative to As(III) (3.3-20 mM), the anions were expected to have an influence on biogenic scorodite crystallization. Therefore, this study focused on the behavior of SO_4^{2-} ions during biogenic scorodite crystallization process via two-stage As-removal.

2. Materials and Methods

2.1. Biogenic scorodite crystallization experiment

Pre-grown *Ac. brierleyi* (DSM 1651) cells were inoculated (to a cell density of 1.0 x 10^7 cells/ml) into 500 ml Erlenmeyer flasks containing 200 ml of heterotrophic basal salts (HBS) medium (pH 1.5 with H_2SO_4; Johnson et al., 2008) with 18 mM (1000 mg/L) Fe^{2+} (as $FeSO_4 \cdot 7H_2O$), 13 mM (1000 mg/l) As(III) (as $NaAsO_2$) and 0.02% (w/v) yeast extract (to set the $[Fe^{2+}]_{ini}/[As(III)]_{ini}$ molar ratio = 1.4), and incubated at 70°C, shaken at 100 rpm. Samples were taken periodically to analyze pH, Eh (vs SHE), cell density (direct count using the Thoma counting chamber) and concentrations of total soluble Fe, As and S (ICP-OES; Optima8300, PerkinElmer), Fe^{2+} (*o*-phenanthroline method) and As(III) (molybdenum blue method). Precipitates were also periodically collected, washed once with distilled water and freeze-dried overnight (FDU-2110, EYELA). All experiments were done in duplicate.

2.2. Effect of different acid media (H_2SO_4, HCl and HNO_3)

In order to investigate the role of SO_4^{2-} ions in formation of amorphous precursors, abiotic comparison tests were conducted with or without the presence of SO_4^{2-}, by using $Fe^{III}_2(SO_4)_3 \cdot nH_2O$, $Fe^{III}Cl_3 \cdot 6H_2O$ or $Fe^{III}(NO_3)_3 \cdot 9H_2O$ as a starting reagent (pH adjusted to 1.5 with H_2SO_4, HCl or HNO_3, respectively) (cf. biotic tests started with $Fe^{II}SO_4 \cdot 7H_2O$ at pH 1.5 with H_2SO_4). Five hundred milliliter Erlenmeyer flasks containing 200 ml of distilled water containing 13 mM (1000 mg/l) As(V) (as $Na_2HAsO_4 \cdot 7H_2O$) plus 18 mM (1000 mg/l) Fe^{3+} using one of the above ferric reagents were prepared and incubated shaken at 70°C and 100 rpm. Experiments were done in duplicates.

2.3. Solid analysis

Chemical compositions of the resultant precipitates (collected on days 3, 5, 6, 7, 8, 9, 10, 11 and 14) were determined by digesting a sample aliquot (50 mg) in 35% HCl, followed by ICP-OES measurement of Fe, As and S concentrations.

Cross-section views of resin-embedded precipitates (epoxy resin; SpeciFix-20, Struers) were observed by SEM (ULTRA55, ZEISS), following polishing (Doctor Lap ML-182, Maruto) and carbon-sputtering (JEC560, JEOL).

In order to understand the behaviors of Fe^{3+}, SO_4^{2-} and AsO_4^{3-} ions during the biogenic scorodite crystallization process, changes in diffuse reflectance FT-IR spectra of As precipitates were followed over time (FT/IR-670, JASCO) by using the KBr pellet method (sample 1% (w/v)). Chemically-synthesized scorodite (Tanaka and Okibe, 2018), freeze-dried *Ac. brierleyi* cells and ferric sulfate n-hydrate ($Fe_2(SO_4)_3{\cdot}nH_2O$, Junsei, extra pure grade) were used as standards. To observe the peaks of H_2O coordinated with Fe^{3+}, 20 mM $FeCl_3{\cdot}6H_2O$ (pH 1.5 with HCl) was used as a standard solution and measured by the attenuated total reflection FTIR spectroscopy (ATR-FTIR) using ZnSe crystal. Broad FTIR peaks at 2500–3600 cm^{-1} were separated by the curve-fitting software PeakFit ver. 4.12 (Systat Software) using the mixed Gaussian and Lorentzian function.

The water content in precipitates was measured by thermogravimetry (TG-DTA 2000SA, Bruker AXS) by heating 5 mg sample in Pt-sample-pan from room temperate to 600°C at 10°C/min with air flow rate of 100 ml/min. The structural water content of the final biogenic scorodite product was calculated based on the weight loss between 125-250°C (Tanaka and Okibe, 2018).

Particles size distribution of As precipitates was measured by laser diffraction

particle size analyzer (LA-950, Horiba).

The chemical formula of the final biogenic scorodite product was determined by the complete chemical digestion and TG analyses.

3. Results and Discussion

3.1. Biogenic scorodite crystallization process via two-stage As-removal (liquid analysis)

In the course of the biogenic scorodite crystallization process (pH 1.5), As precipitation occurred typically in two-stages with an induction period between the two stages (Okibe et al. 2017; Tanaka and Okibe, 2018). *Ac. brierleyi* was adapted over years to As(III), which resulted in the archaeon's current ability in a fast As(III) oxidation (cf. Okibe et al., 2014, 2017; Tanaka and Okibe, 2018).

Fig.1 shows microbial oxidation of As(III) (Fig. 1a) and Fe^{2+} (Fig. 1ab) triggering immobilization of As (Fig. 1a) and Fe (Fig. 1b) in relation to changes in the SO_4^{2-} concentration (Fig. 1c), pH and cell density (Fig. 1d) over time. The first-stage As-removal was seen between days 1-5 where 8 mM As (Fig. 1a) and 11.5 mM Fe (Fig. 1b) were immobilized together with 2.5 mM SO_4^{2-} (Fig. 1c) ($\Delta[As]_{liq}$:$\Delta[Fe]_{liq}$:$\Delta[SO_4^{2-}]_{liq}$ = 0.69:1:0.22), producing brown-colored amorphous precipitates. The next induction period of constant concentration (days 5-11) was followed by the second-stage As-removal between days 11-15, where 4.5 mM As (Fig. 1a) and 2.5 mM Fe (Fig. 1b) were immobilized together with 1 mM SO_4^{2-} (Fig. 1c) from the bulk solution ($\Delta[As]_{liq}$:$\Delta[Fe]_{liq}$:$\Delta[SO_4^{2-}]_{liq}$ = 1.8:1:0.4). During this second-stage, the color of precipitates turned from brown to pale-green overnight with removal of 98% As by day 15 (Fig. 1a). Overall, between days 0-15, 12.5 mM As (Fig. 1a), 14 mM Fe (Fig. 1b) and 3.5 mM SO_4^{2-} (Fig. 1c) were immobilized ($\Delta[As]_{liq}$:$\Delta[Fe]_{liq}$:$\Delta[SO_4^{2-}]_{liq}$ = 0.89:1:0.25).

The finding that excess Fe relative to As was immobilized in the first-stage while less Fe was in the second-stage implied that Fe immobilized in the first-stage was

somehow re-supplied to transform initial amorphous precursors into the final product of crystalline biogenic scorodite.

3.2. Incorporation of SO_4^{2-} ions in amorphous precursors (solid digestion)

To understand the transformation process, the immobilized solid phase was collected periodically, digested in 35% HCl and analyzed for their chemical compositions.

Based on the solid digestion, the first-stage As-removal (days 1-5) produced amorphous precipitates corresponding to $[AsO_4^{3-}]_{im}/[Fe]_{im}$ = 0.74-0.77 and $[SO_4^{2-}]_{im}/[Fe]_{im}$ = 0.15-0.20 (Fig. 2). The amorphous precursors formed by day 5 was thus calculated to have $[As]_{im}:[Fe]_{im}:[SO_4^{2-}]_{im}$ = 0.77:1:0.15 (cf. $\Delta[As]_{liq}:\Delta[Fe]_{liq}:\Delta[SO_4^{2-}]_{liq}$ = 0.69:1:0.22; calculated from the liquid phase in section 3.1). This excess immobilization of Fe versus As suggested that amorphous precursors do not comprise solely of amorphous scorodite with the theoretical molar ratio Fe/As=1.

Following the induction period (days 5-11), the second-stage As-removal (days 11-15) led to a decrease in $[SO_4^{2-}]_{im}/[Fe]_{im}$ from 0.20 to 0.08. This was accompanied by an increase in $[AsO_4^{3-}]_{im}/[Fe]_{im}$ from 0.74 to 0.94, becoming closer to the theoretical molar ratio Fe/As=1 for scorodite (Fig. 2). It was calculated based on the solid analysis that the final crystalline biogenic scorodite product formed by day 15 had $[As]_{im}:[Fe]_{im}:[SO_4^{2-}]_{im}$ = 0.94:1:0.08 (cf. $\Delta[As]_{liq}:\Delta[Fe]_{liq}:\Delta[SO_4^{2-}]_{liq}$ = 0.89:1:0.25; calculated from the liquid phase in section 3.1). It should be noted that reliability in the quantification of liquid-phase SO_4^{2-} is relatively low due to a small difference in the concentration.

In consistence with the liquid-phase observations (section 3.1), the results from

the solid digestion again suggested that Fe immobilized in the first-stage as amorphous precursors was released and re-supplied during the second-stage As-removal to eventually crystalize final biogenic scorodite.

3.3. Abiotic comparison tests in H_2SO_4, HCl and HNO_3 media

Since the incorporation of SO_4^{2-} ions into amorphous biogenic scorodite precursors was suggested, different acid media (H_2SO_4, HCl and HNO_3) were compared to confirm the role of SO_4^{2-} in simple abiotic tests using an oxidized form of As(V) (13 mM) and Fe^{3+} (18 mM) as starting reagents. Fig. 3 shows that neither As nor Fe was precipitated in HCl and HNO_3 media, but the use of H_2SO_4 medium indeed triggered the rapid precipitation of brown amorphous precursors within 1 hour, which then transformed to crystalline scorodite (pale-green) after day 4. The same trend was observed when started from As(V) (26 mM) and Fe^{3+} (36 mM) (data, not shown). A negative effect of SO_4^{2-} ions was previously reported in chemical scorodite synthesis where conditions used were more favorable for scorodite crystallization kinetics (e.g., Demopoulos et al., 1995). In contrast, under dilute As concentrations and lower temperature conditions (such as in this study), initial precipitation of SO_4^{2-}-containing precursors may become a key to trigger their subsequent transformation to crystalline scorodite. The underlying mechanism was thus further investigated as follows.

3.4. Phase transformation from amorphous precursors to crystalline biogenic scorodite (FT-IR and TG analyses)

Fig. 4 shows overtime changes in FT-IR spectra of precipitates collected at different time points. Two bands at 1060 and 1121 cm^{-1} (Fig. 4), corresponding to SO_4^{2-}

interacting with Fe^{3+} and OH^- ions (1058 and 1112 cm^{-1}; Powers et al., 1975), were present in initial amorphous precursors (day 3) and gradually disappeared by day 11. This was correlated with transformation of a single broad band (2500–3650 cm^{-1}, corresponding to OH stretching vibrations in hydration H_2O molecules; Jia et al., 2007) to two distinctive bands (sharp 3525 cm^{-1} and broad 2976 cm^{-1}, deriving from scorodite hydration H_2O molecules; sharp 3511 cm^{-1}, broad 2927 cm^{-1}; Baghurst et al. 1996). The intensity of two bands at 422 and 827 cm^{-1}, corresponding to AsO_4^{3-} stretching vibrations in scorodite (436 and 825 cm^{-1}; Ondrus et al. 1999) were mostly unchanged, of which the slightly broad band at 827 cm^{-1} on (day 3 gradually turned into a sharp peak, likely due to the disappearance of two OH deformation bands at both shoulders, indicating the cleavage of Fe-OH bond (Ruan et al., 2002). The peaks at 1541 and 1649 cm^{-1} were attributed to cell proteins (1545 and 1654 cm^{-1}; Legal et al. 1991).

For further understandings, the above mentioned broad bands (2500–3650 cm^{-1}) from samples (days 5, 9 and 14) and standards ($FeAsO_4 \cdot 2H_2O$ and $Fe_2(SO_4)_3 \cdot nH_2O$) were subjected to peak separation (Fig. 5) and the resultant peaks were assigned in Table 1. The peaks at 3182, 3337 and 3465 cm^{-1} (day 5; Fig. 5a), representing H_2O coordinated with Fe^{3+}-SO_4^{2-} compounds, progressively disappeared towards the completion of crystallization. Instead, a clear peak at 3523 cm^{-1} (day 14; Fig. 5c) (corresponding to the Fe^{3+}-H_2O band in crystalline scorodite) became visible by day 14. At the same time, the peak at 2984 cm^{-1} (deriving from H_2O coordinated with crystalline scorodite) emerged to represent the top of the broad peak (day 14; Fig.5c).

Overall, transformation process of amorphous precursors to crystalline biogenic scorodite involved the disappearance of SO_4^{2-} and Fe-OH bands while retaining AsO_4^{3-} bands. Therefore, it can be considered that the amorphous precursors

formed during the first As-removal stage consist of at least two types of precipitates ($Fe–SO_4$ compounds and $Fe–AsO_4$ compounds), most likely in this case, basic ferric sulfate ($MFe_x(SO_4)_y(OH)_z$; M^+ = K^+, Na^+, NH_4^+) and amorphous ferric arsenate ($FeAsO_4 \cdot (2+n)H_2O$; Le Berre et al., 2008).

According to TG-DTA analysis (Fig. 6), a continuous weight loss was observed for amorphous precursors (days 5-9) during heating, as was also the case for previously reported basic ferric arsenate sulfate ($Fe(AsO_4)_{1-x}(SO_4)_x(OH)_x \cdot wH_2O$; hydrothermally synthesized by Gomez et al., 2011), poorly-crystalline ferric arsenate ($Fe_{1.07}AsO_4 \cdot 3.06H_2O$; atmospherically synthesized by Le Berre et al., 2007) and basic ferric sulfate ($Fe(OH)SO_4$; Dutrizac and Jambor, 2007). The amount of weight loss (before reaching 550°C) decreased at later sampling days (21.4% on day 5, 19.7% on day 7, 18.9% on day 8, 18.3% on day 9), indicating that dehydration also accompanied phase transformation of amorphous precursors to the final crystalline biogenic scorodite. Together with the chemical digestion result, the chemical formula of the final biogenic scorodite product from this study was calculated to be $Fe(AsO_4)_{0.94}(SO_4)_{0.08} \cdot 1.69H_2O$.

3.5. Dissolution-recrystallization of SO_4^{2-}-bearing amorphous precursors triggers biogenic scorodite crystallization

SEM observation (Fig. 7) revealed that round amorphous precursors formed in the first As-removal stage were filled particles (day 3; Fig. 7a, e). During the next induction period, the formation of secondary mineral layers became increasingly visible on the surface of amorphous precursors (days 7-8; Fig. 7b, c, f, h). Here, the least stable phase (mainly amorphous basic ferric sulfate (cf. $K_{sp} = 10^{-11.0}$ for jarosite; Baron and Palmer, 1996) and amorphous ferric arsenate ($K_{sp} = 10^{-23.0}$; Langmuir et al., 2006))

precipitated first, which was followed by their dissolution-recrystallization equilibrium to gradually transform amorphous precursors into crystalline scorodite. The length of the induction period is thus initially dictated by the time needed for re-dissolved metal ions to become locally and sufficiently concentrated on the surface of amorphous precursors, which gives the first driving force to form a crystalline scorodite layer. Since the layer structure is porous and partially discontinuous (Fig. 7 g, h), soluble metal ions may move across the scorodite layer. However, crystalline biogenic scorodite serves as absorbent for free As(V) anions (Okibe, unpublished data) due to its surface potential (~50 mV at pH 2.0; Okibe et al., 2017), whilst amorphous particles do not (~25 mV at pH 2.0; Okibe et al., 2017). This electrostatic effect is also expected to be an additional driving force to push further scorodite crystallization on the sides of the scorodite layer, eventually leaving only the "shell" structure (day 14; Fig. 7d, h).

During this transformation process, alteration of the above-mentioned particle surface potential (from ~25 mV to ~50 mV at pH 2.0; Okibe et al., 2017) also led to a change in the particle size: The particle size distribution of amorphous precursors was non-uniform and ranged widely between 4 to 200 μm (likely due to partial aggregation owing to their lower surface charge; Fig. 8), while that of the final crystalline product showed a more uniform particle size with the average of 36.9 μm (due to enhanced electrostatic repulsive force) (Fig. 8). Although the resultant biogenic scorodite products are hollow particles, they were shown to be excellent seed-crystals for further biogenic scorodite accumulation with sufficient stability (Tanaka and Okibe, 2018).

According to this dissolution-recrystallization mechanism, the different As-removal behavior observed at pH 1.2 (single-stage As-removal, seemingly directly as crystalline biogenic scorodite; Tanaka and Okibe, 2018), compared to the two-stage

As-removal at pH 1.5, can be explained by the different behavior of amorphous precursors: The immediate dissolution of amorphous precursors under more acidic pH (Baron and Palmer, 1995; Smith et al., 2006; Welch et al., 2008) likely led to apparent diminishment of the inducing period. However, compared to relatively incomplete As-removal at pH 1.2 (Tanaka and Okibe, 2018), the two-stage As-removal via SO_4^{2-}-mediated phase transformation was indeed found to play an important role in effective biogenic scorodite crystallization.

4. Conclusions

Based on the overall findings, a mechanism of the biogenic scorodite crystallization process is proposed in Fig. 9.

First, microbial oxidation of Fe^{2+} and As(III) [Eq. 3 and 4, respectively] proceed readily, triggering the first-stage As-removal as amorphous precursors composed of basic ferric sulfate [Eq. 5] and ferric arsenate [Eq. 6] (Phase I):

$4Fe^{2+} + O_2 + 4H^+ = Fe^{3+} + 2H_2O$ (biological) [Eq. 3]

$2H_3As^{III}O_3 + O_2 = 2H_2As^{V}O_4^- + 2H^+$ (biological) [Eq. 4]

$M^+ + xFe^{3+} + yHSO_4^- + zH_2O = MFe_x(SO_4)_y(OH)_{z\ (amorphous)} + (y+z)H^+$ [Eq. 5]

($M^+ = K^+, Na^+, NH_4^+$)

$Fe^{3+} + H_2AsO_4^- + (2+n)H_2O = FeAsO_4{\cdot}(2+n)H_2O_{(amorphous)} + 2H^+$ [Eq. 6]

During the induction period, the dissolution-recrystallization process takes place for phase transformation according to the Stranski's rule (the order of solubility S(A)>S(B)>S(C) follows the order of initial precipitation rates $R_A>R_B>R_C$; Blesa and Matijevic, 1989; Demopoulos, 2009). In this case, the least stable phase (mainly amorphous basic ferric sulfate and amorphous ferric arsenate precipitate first, followed

by their dissolution-recrystallization (Phase II). By doing so metal ions become locally concentrated on the precursors surface which gives the driving force for crystallization of secondary layers of biogenic scorodite (K_{sp} = $10^{-25.8}$; Langmuir et al., 2006), from even very dilute and seeded aqueous environment [Eq. 7, 8] (Phase III). This phase transformation is also accompanied by a dehydration process.

$FeAsO_4 \cdot (2+n)H_2O_{(amorphous)} = FeAsO_4 \cdot 2H_2O_{(crystalline)} + nH_2O$ [Eq.7]

$Fe^{3+} + H_2AsO_4^- + 2H_2O = FeAsO_4 \cdot 2H_2O_{(crystalline)} + 2H^+$ [Eq.8]

(cf., chemical formula of biogenic scorodite product in this study was calculated to be $Fe(AsO_4)_{0.94}(SO_4)_{0.08} \cdot 1.69H_2O$)

This two-stage As-removal via SO_4^{2-}-mediated phase transformation was found to play an important role in effective biogenic scorodite crystallization.

Acknowledgement

This work was partly supported by JSPS KAKENHI (Grant Number JP24760689). M.T. is grateful for the financial assistance provided by the Kyushu University Advanced Graduate Program in Global Strategy for Green Asia.

References

Baghurst, D.R., Barret, J., Coleyshaw, E.E., Griffith, W.P., Mingos, D.M.P., 1996. Microwave techniques for the synthesis and deuteration of minerals, with particular reference to scorodite, $FeAsO_4 \cdot 2H_2O$, Mineral. Mag., 821.

Baron, D., Palmer, C.D., 1996. Solubility of jarosite at 4–35 °C. Geochim. Cosmochim. Ac. 60 (2), 185-195.

Blesa, M.A., Matijević, E., 1989. Phase transformations of iron oxides, oxohydroxides, and hydrous oxides in aqueous media. Adv. Colloid Interfac. 29 (3), 173-221.

Demopoulos, G.P., Droppert, D.J., Van Weert, G., 1995. Precipitation of crystalline scorodite ($FeAsO_4 \cdot 2H_2O$) from chloride solutions. Hydrometallurgy 38 (3), 245-261.

Demopoulos, G.P., 2009. Aqueous precipitation and crystallization for the production of particulate solids with desired properties. Hydrometallurgy 96 (3), 199-214.

Dutrizac, J.E., Jambor, J.L., 1988. The synthesis of crystalline scorodite, $FeAsO_4 \cdot 2H_2O$. Hydrometallurgy 19 (3), 377-384.

Dutrizac, J.E., Jambor, J.L., 2007. Characterization of the iron arsenate–sulphate compounds precipitated at elevated temperatures. Hydrometallurgy 86 (3), 147-163.

EPA, 1992. EPA Method 1311. Toxicity Characteristic Leaching Procedure. Test

methods for evaluating solid wastes physical/chemical methods. United States Environmental Protection Agency, Washington DC.

Filippou, D., Demopoulos, G.P., 1997. Arsenic immobilization by controlled scorodite precipitation. JOM 49 (12), 52-55.

Fujita, T., Taguchi, R., Abumiya, M., Matsumoto, M., Shibata, E., Nakamura, T., 2008a. Novel atmospheric scorodite synthesis by oxidation of ferrous sulfate solution. Part I. Hydrometallurgy 90 (2–4), 92-102.

Fujita, T., Taguchi, R., Abumiya, M., Matsumoto, M., Shibata, E., Nakamura, T., 2008b. Novel atmospheric scorodite synthesis by oxidation of ferrous sulfate solution. Part II. Effect of temperature and air. Hydrometallurgy 90 (2–4), 85-91.

Fujita, T., Taguchi, R., Abumiya, M., Matsumoto, M., Shibata, E., Nakamura, T., 2009. Effect of pH on atmospheric scorodite synthesis by oxidation of ferrous ions: Physical properties and stability of the scorodite. Hydrometallurgy 96 (3), 189-198.

Gomez, M.A., Becze, L., Cutler, J.N., Demopoulos, G.P., 2011. Hydrothermal reaction chemistry and characterization of ferric arsenate phases precipitated from $Fe_2(SO_4)_3$–As_2O_5–H_2SO_4 solutions. Hydrometallurgy 107 (3), 74-90.

Jia, Y., Xu, L., Wang, X., Demopoulos, G.P., 2007. Infrared spectroscopic and X-ray diffraction characterization of the nature of adsorbed arsenate on ferrihydrite. Geochim.

Cosmochim. Ac. 71 (7), 1643-1654.

Johnson, D.B., Joulian, C., d'Hugues, P., Hallberg, K.B., 2008. *Sulfobacillus benefaciens* sp. nov., an acidophilic facultative anaerobic *Firmicute* isolated from mineral bioleaching operations. Extremophiles 12 (6), 789-798.

Langmuir, D., Mahoney, J., Rowson, J., 2006. Solubility products of amorphous ferric arsenate and crystalline scorodite ($FeAsO_4 \cdot 2H_2O$) and their application to arsenic behavior in buried mine tailings. Geochim. Cosmochim. Ac. 70 (12), 2942-2956.

Le Berre, J.F., Gauvin, R., Demopoulos, G.P., 2007. Characterization of poorly-crystalline ferric arsenate precipitated from equimolar Fe(III)-As(V) solutions in the pH range 2 to 8. Metall. Mater. Trans. B 38 (5), 751-762.

Le Berre, J.F., Gauvin, R., Demopoulos, G.P., 2008. A study of the crystallization kinetics of scorodite via the transformation of poorly crystalline ferric arsenate in weakly acidic solution. Colloid. Surface. A 315 (1), 117-129.

Legal, J.M., Manfait, M., Theophanides, T., 1991. Applications of FTIR spectroscopy in structural studies of cells and bacteria. J. Mol. Struct. 242, 397-407.

Monhemius, A.J., Swash, P.M., 1999. Removing and stabilizing as from copper refining circuits by hydrothermal processing. JOM 51 (9), 30-33.

Myneni, S.C.B., Traina, S.J., Waychunas, G.A., Logan, T.J., 1998. Vibrational spectroscopy of functional group chemistry and arsenate coordination in ettringite. Geochim. Cosmochim. Ac. 62 (21), 3499-3514.

Okibe, N., Koga, M., Sasaki, K., Hirajima, T., Heguri, S., Asano, S., 2013. Simultaneous oxidation and immobilization of arsenite from refinery waste water by thermoacidophilic iron-oxidizing archaeon, *Acidianus brierleyi*. Miner. Eng. 48, 126-134.

Okibe, N., Koga, M., Morishita, S., Tanaka, M., Heguri, S., Asano, S., Sasaki, K., Hirajima, T., 2014. Microbial formation of crystalline scorodite for treatment of As(III)-bearing copper refinery process solution using *Acidianus brierleyi*. Hydrometallurgy 143, 34-41.

Okibe, N., Morishita, S., Tanaka, M., Sasaki, K., Hirajima, T., Hatano, K., Ohata, A., 2017. Bioscorodite crystallization using *Acidianus brierleyi*: Effects caused by Cu(II) present in As(III)-bearing copper refinery wastewaters. Hydrometallurgy 168, 121-126.

Ondruš, P., Skála, R., Viti, C., Veselovský, F., Novák, F., Jansa, J., 1999. Parascorodite, $FeAsO_4 \cdot 2H_2O$—a new mineral from Kaňk near Kutná Hora, Czech Republic, Am. Mineral., 1439.

Powers, D.A., Rossman, G.R., Schugar, H.J., Gray, H.B., 1975. Magnetic behavior and infrared spectra of jarosite, basic iron sulfate, and their chromate analogs. J. Solid State

Chem. 13 (1), 1-13.

Riveros, P.A., Dutrizac, J.E., Spencer, P., 2001. Arsenic disposal practices in the metallurgical industry. Can. Metall. Q. 40 (4), 395-420.

Ruan, H.D., Frost, R.L., Kloprogge, J.T., Duong, L., 2002. Infrared spectroscopy of goethite dehydroxylation: III. FT-IR microscopy of in situ study of the thermal transformation of goethite to hematite. Spectrochim. Acta A 58 (5), 967-981.

Singhania, S., Wang, Q., Filippou, D., Demopoulos, G.P., 2005. Temperature and seeding effects on the precipitation of scorodite from sulfate solutions under atmospheric-pressure conditions. Metall. Mater. Trans. B 36 (3), 327-333.

Singhania, S., Wang, Q., Filippou, D., Demopoulos, G.P., 2006. Acidity, valency and third-ion effects on the precipitation of scorodite from mixed sulfate solutions under atmospheric-pressure conditions. Metall. Mater. Trans. B 37 (2), 189-197.

Smith, A.M.L., Hudson-Edwards, K.A., Dubbin, W.E., Wright, K., 2006. Dissolution of jarosite [$KFe_3(SO_4)_2(OH)_6$] at pH 2 and 8: Insights from batch experiments and computational modelling. Geochim. Cosmochim. Ac. 70 (3), 608-621.

Tanaka, M., Okibe, N., 2018. Factors to enable crystallization of environmentally stable bioscorodite from dilute As(III)-contaminated waters. Minerals 8 (1), 23.

Welch, S.A., Kirste, D., Christy, A.G., Beavis, F.R., Beavis, S.G., 2008. Jarosite dissolution II—Reaction kinetics, stoichiometry and acid flux. Chem. Geol. 254 (1), 73-86.

Figure and Table Legends

Fig. 1 Changes in concentrations of; (a) total soluble As (●) or As(III) (○), (b) total soluble Fe (●) or Fe^{2+} (○), (c) soluble SO_4^{2-} and (d) cell density (●) or pH (○) in *Ac. brierleyi* cultures ($[As(III)]_{ini}$ = 13 mM, $[Fe^{2+}]_{ini}$ = 18 mM, pH 1.5, 70°C). Grey dotted lines indicate the periods for the first-stage As-removal, induction (constant concentration) and the final second-stage As-removal.

Fig. 2 Changes in the chemical composition of As precipitates periodically collected from *Ac. brierleyi* cultures (from Fig. 1), expressed as molar ratios of immobilized AsO_4^{3-} over immobilized Fe ($[AsO_4]_{im}/[Fe]_{im}$; ●) and immobilized SO_4^{2-} over immobilized Fe ($[SO_4]_{im}/[Fe]_{im}$; ○). Grey dotted lines indicate the periods for the first-stage As-removal, induction (constant concentration) and the final second-stage As-removal.

Fig. 3 Comparison of different acid media (●, H_2SO_4; ■, HCl; ▲, HNO_3) for abiotic scorodite formation ($[As(V)]_{ini}$ = 13 mM, $[Fe(III)]_{ini}$ = 18 mM, pH 1.5, 70°C). (a) total soluble As, (b) total soluble Fe and (c) soluble SO_4^{2-}.

Fig. 4 Overtime changes in FT-IR spectra and color of As precipitates (day 3, 5, 8, 9, 10, 11, 14) (a). Chemical scorodite (b), *Ac. brierleyi* dry cells (c), ferric sulfate n-hydrate (d), aqueous Fe^{3+} (e) and aqueous SO_4^{2-} were measured as standards.

Fig. 5 Curve fitted FT-IR spectra of the OH stretching vibration bands (2500–3700 cm^{-1}) of hydration H_2O molecules. As precipitates (day 5 (a); day 9 (b); day 14 (c)) and

standard samples (chemical scorodite (d) and ferric sulfate n-hydrate (e)) were analyzed using the mixed Gaussian and Lorentzian function. Peak assignments are summarized in Table 1.

Fig. 6 TG analysis of As precipitates periodically collected from *Ac. brierleyi* cultures on day 5 (dashed line), day 7 (dashed dotted line), day 8 (dashed double-dotted line), day 9 (dotted line) and day 14 (solid line).

Fig. 7 SEM images of As precipitates collected on day 3 (a,e), day 7 (b, f), day 8 (c, g) and day 14 (d, h) at 5000× (surface-view; a-d) or 1000× (cross-section view; e-h) magnification.

Fig. 8 Particle size distribution of As precipitates collected from *Ac. brierleyi* cultures on day 3 (dotted line), day 7 (dash-dotted line), day 10 (dash-double-dotted line) and day 14; solid line).

Fig. 9 Schematic illustration of biogenic scorodite crystallization process via SO_4^{2-}-mediated phase transformation by using *Ac. brierleyi* at pH 1.5.

Table 1 Summary of FT-IR peak assignments (OH stretching vibration bands in hydration H_2O molecules; Fig. 5).

Samples						Standards				Peak assignment	Reference
Day 5		Day 9		Day 14		$FeAsO_4 \cdot 2H_2O$		$Fe_2(SO_4)_3 \cdot nH_2O$			
Ob	Se	Ob	Se	Obs	Se	Obs	Se	Obs	Se	H_2O	

served	parated	served	parated	erved	parated	erved	parated	erved	parated	coordinated with:		
2500-3650 (broad, peak at 3108)	2600 2701 2835 2991	2600-3650 (broad, peak at 3059)	2600 2702 2842 3000	2500-3450 (broad, peak at 2976)	2602 2708 2821 2984	2500-3450 (broad, peak at 2966)	2579 2667 2757 2948	2500-3650 (broad, peak at 3242)	- - - -	- - - -	- - - -	
	3182		3185		3180		3178		3178	Fe^{3+}	3 1 7 4	This study (Fig. 4e)
	3337		3328		-		-		3295	SO_4^{2-}	3 3 0 2	This study (Fig. 4f); Myneni et al., 1998
	3465		3444		3523 (sharp) 3561 (sharp)		3516 (sharp)		3551	SO_4^{2-} Fe^{3+}	3 4 6 0 3 5 2 5	This study (Fig. 4f); Myneni et al., 1998 This study (Fig. 4b, e)

Highlights

- As removed as bioscorodite in two-stages with an induction period between the two
- SO_4^{2-}-bearing amorphous precursors form first (1^{st}-stage)
- Amorphous precursors consist of basic ferric sulfate and ferric arsenate
- Precursors dissolution-recrystallization triggers scorodite crystallization (2^{nd}-stage)
- SO_4^{2-}-mediated phase transformation is the key to greater final As-removal

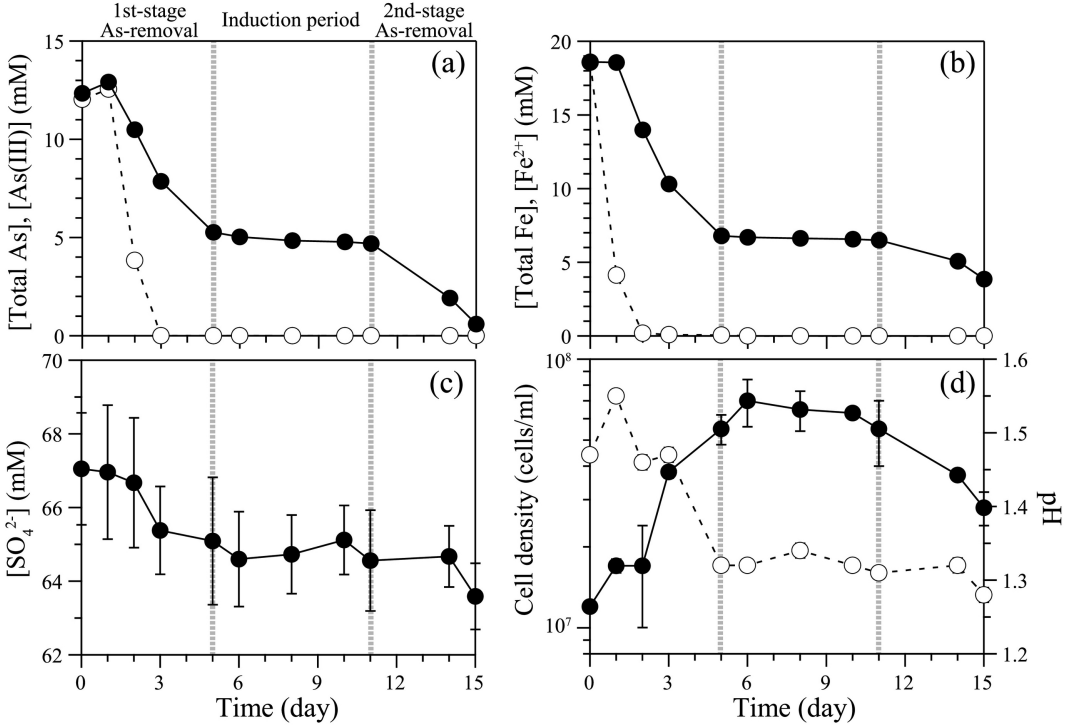
1st-stage
As-removal
Induction period
2nd-stage
As-removal
(a)
[Total As], [As(III)] (mM)
(b)
[Total Fe], [Fe2+] (mM)
(c)
[SO4 2-] (mM)
(d)
Cell density (cells/ml)
pH
Time (day)
Time (day)

Figure 1

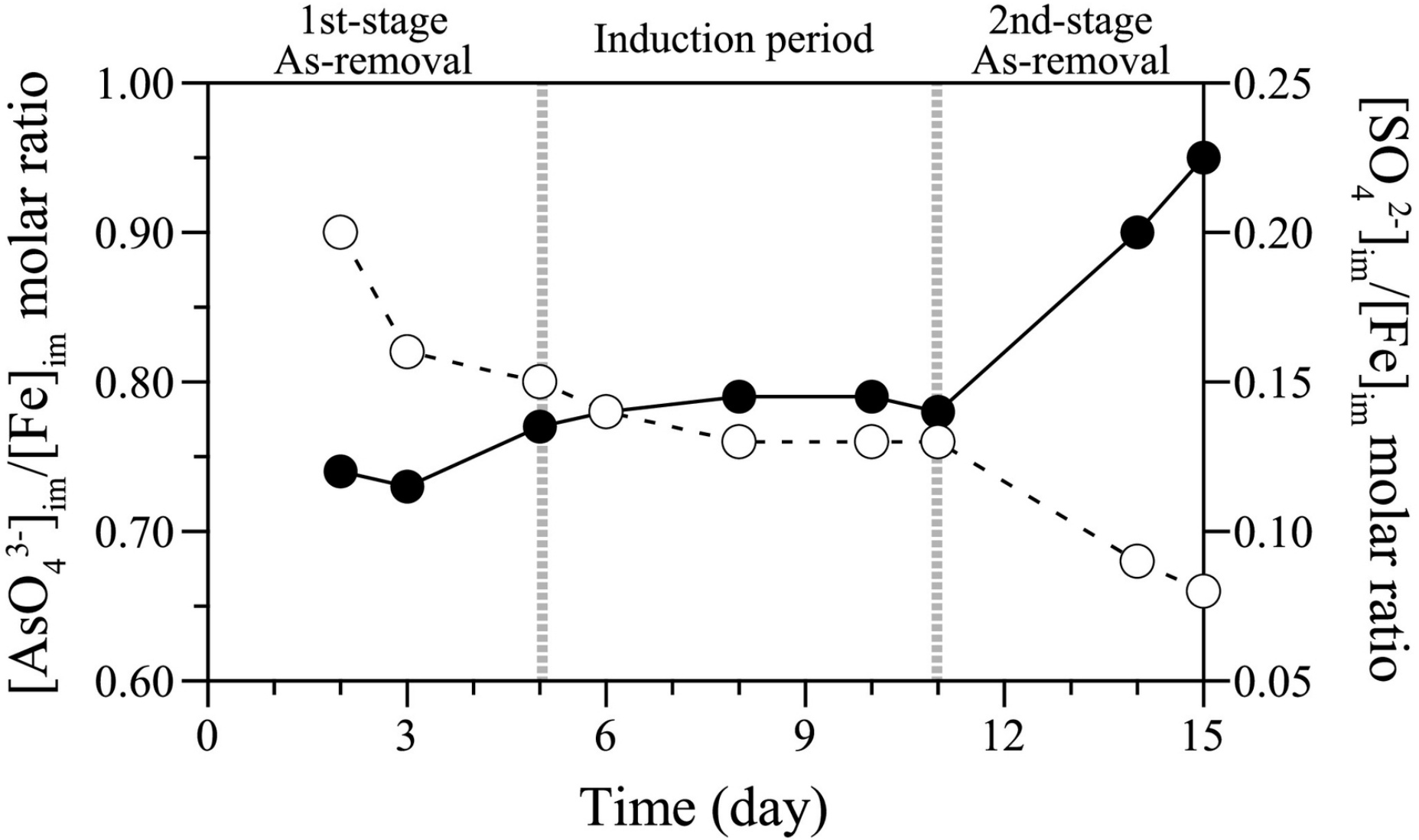
1st-stage
As-removal
Induction period
2nd-stage
As-removal
1.00
0.90
0.80
0.70
0.60
0.25
0.20
0.15
0.10
0.05
0
3
6
9
12
15
Time (day)
[AsO4 3-]im/[Fe]im molar ratio
[SO4 2-]im/[Fe]im molar ratio

Figure 2

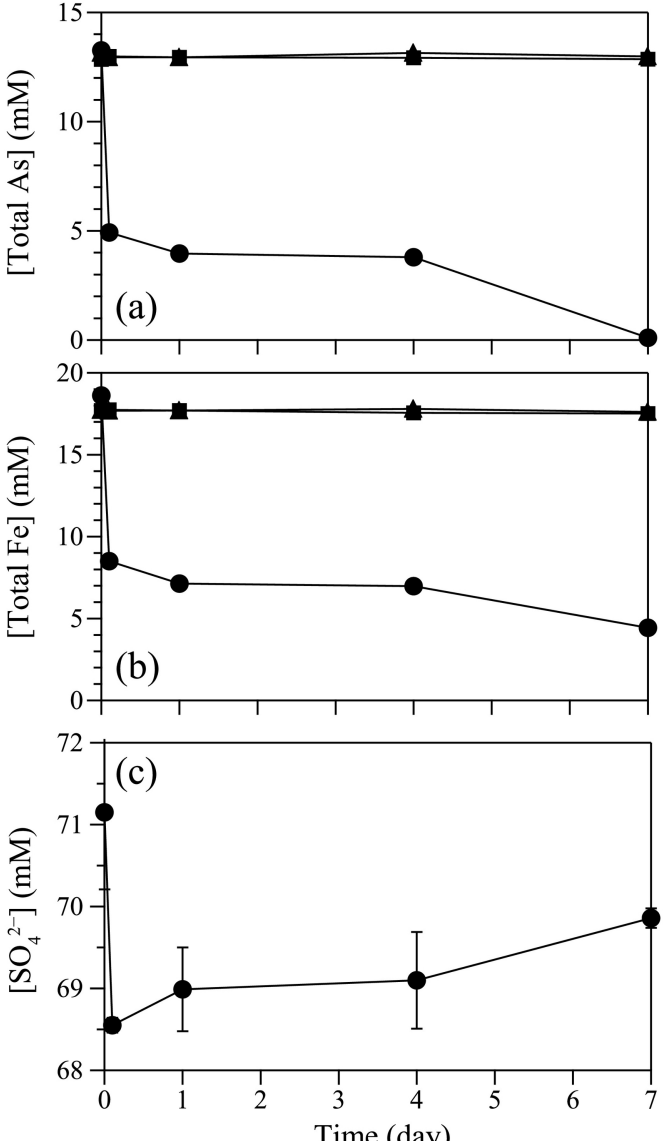
[Total As] (mM)
15
10
5
0
(a)
[Total Fe] (mM)
20
15
10
5
0
(b)
$[SO_4^{2-}]$ (mM)
72
71
70
69
68
(c)
0
1
2
3
4
5
6
7
Time (day)

Figure 3

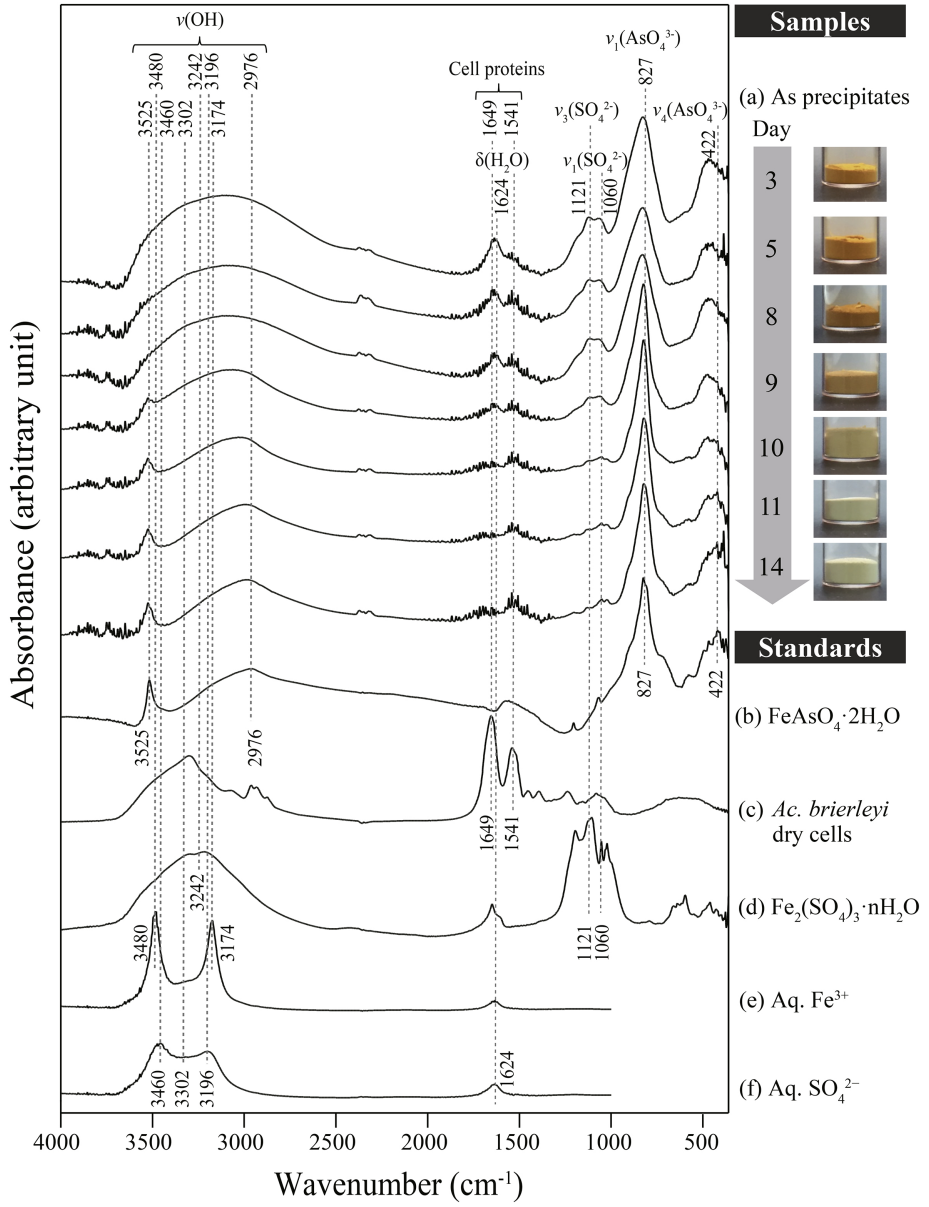
Samples
(a) As precipitates
Day
3
5
8
9
10
11
14
Standards
(b) FeAsO4·2H2O
(c) Ac. brierleyi dry cells
(d) Fe2(SO4)3·nH2O
(e) Aq. Fe3+
(f) Aq. SO4 2−
ν(OH)
3525
3480
3460
3302
3242
3196
3174
2976
Cell proteins
1649
1541
δ(H2O)
1624
ν3(SO4 2-)
ν1(SO4 2-)
1121
1060
ν1(AsO4 3-)
827
ν4(AsO4 3-)
422
Absorbance (arbitrary unit)
4000
3500
3000
2500
2000
1500
1000
500
Wavenumber (cm-1)

Figure 4

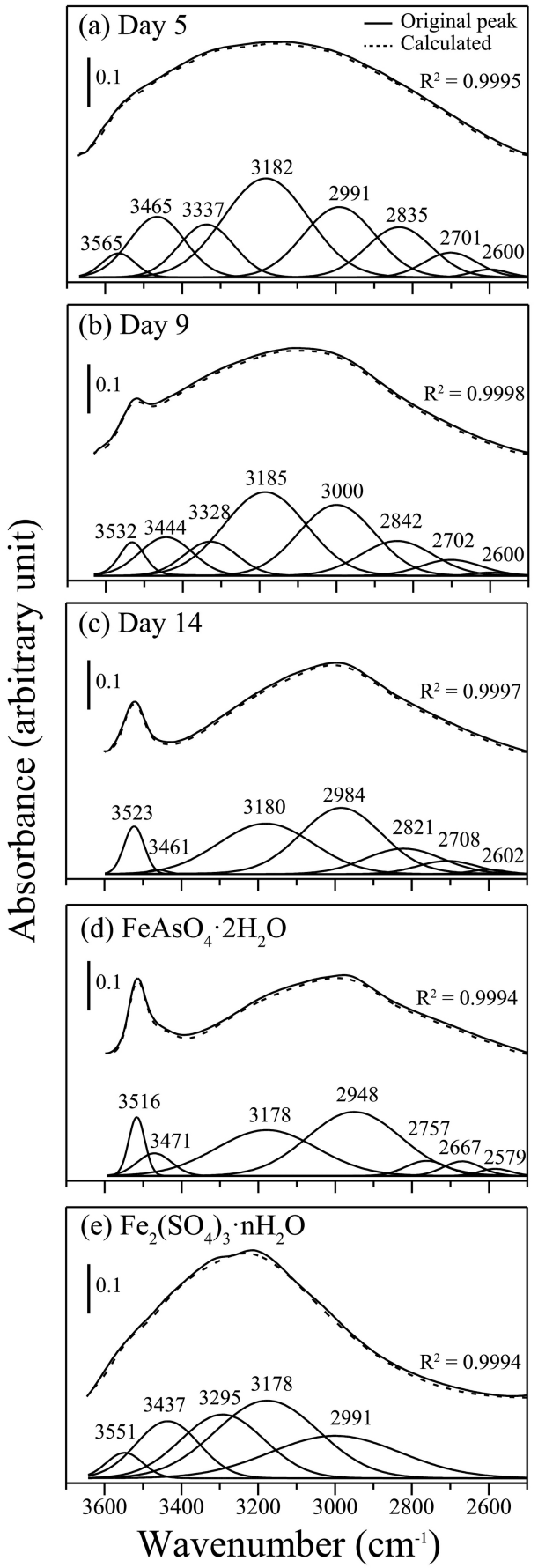
(a) Day 5
Original peak
Calculated
0.1
R² = 0.9995
3565
3465
3337
3182
2991
2835
2701
2600
(b) Day 9
0.1
R² = 0.9998
3532
3444
3328
3185
3000
2842
2702
2600
(c) Day 14
0.1
R² = 0.9997
3523
3461
3180
2984
2821
2708
2602
(d) FeAsO4·2H2O
0.1
R² = 0.9994
3516
3471
3178
2948
2757
2667
2579
(e) Fe2(SO4)3·nH2O
0.1
R² = 0.9994
3551
3437
3295
3178
2991
Absorbance (arbitrary unit)
3600
3400
3200
3000
2800
2600
Wavenumber (cm-1)

Figure 5

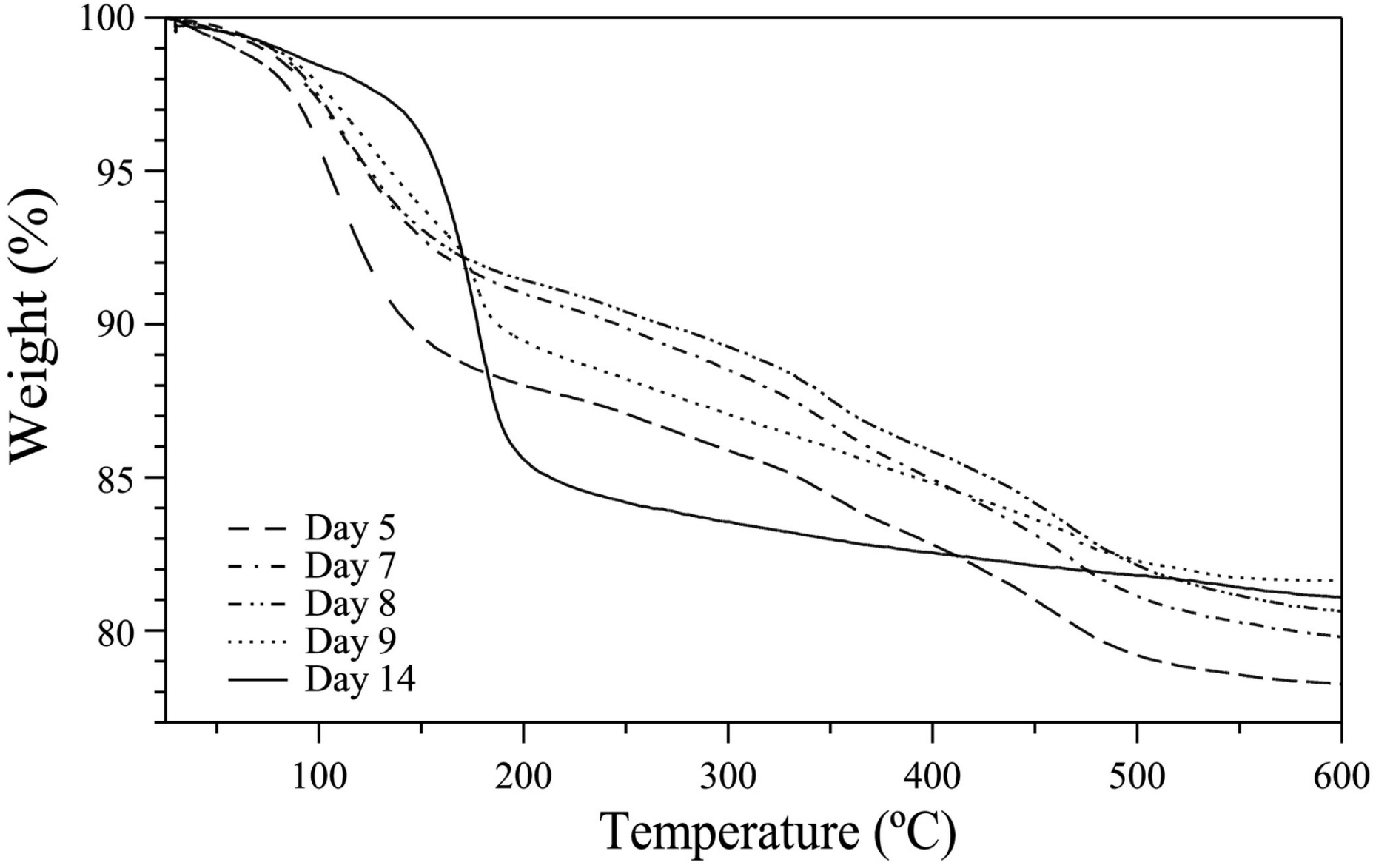
100
95
90
85
80
Weight (%)
Day 5
Day 7
Day 8
Day 9
Day 14
100
200
300
400
500
600
Temperature (ºC)

Figure 6

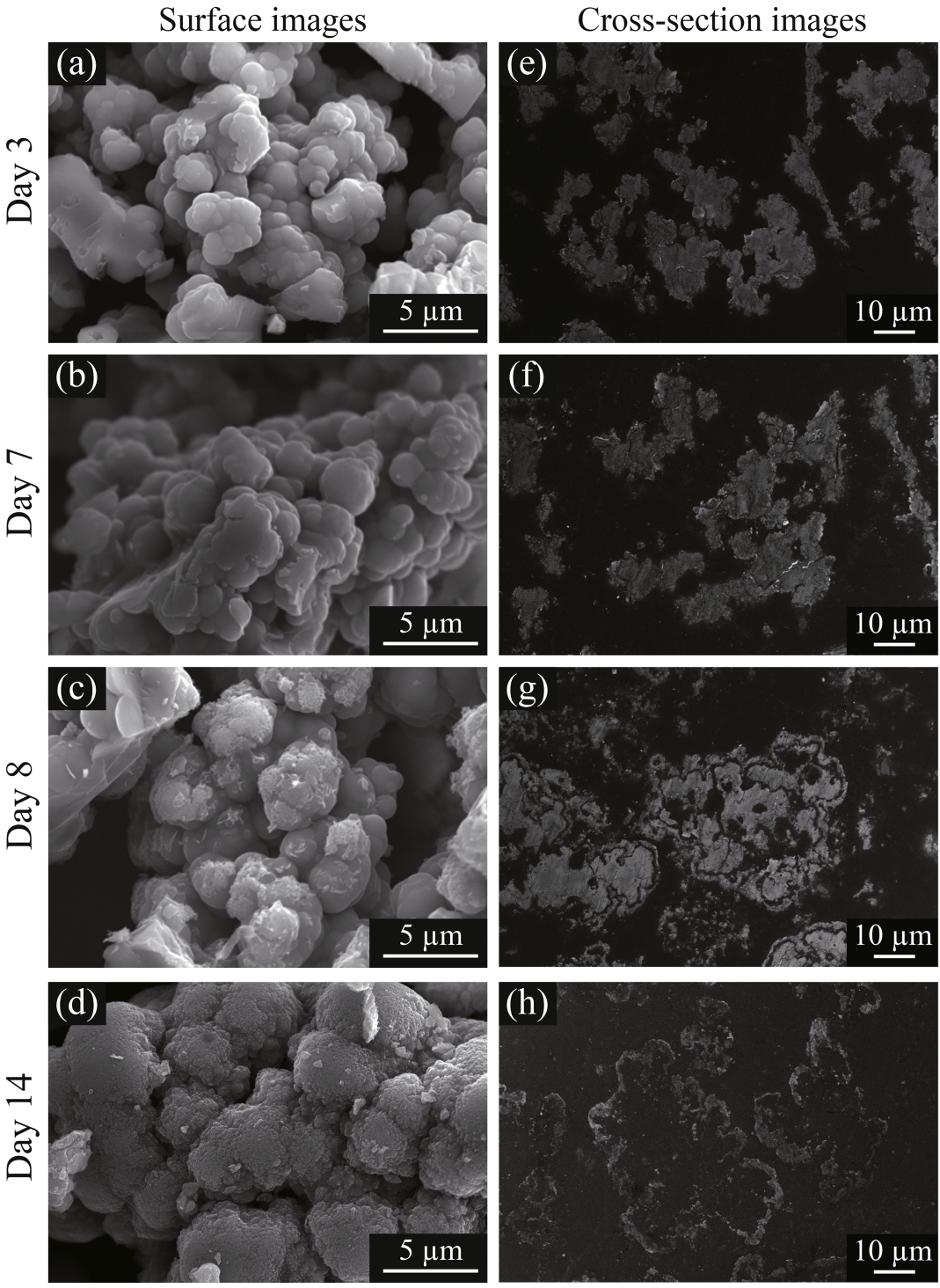
Surface images
Cross-section images
Day 3
Day 7
Day 8
Day 14
(a)
(b)
(c)
(d)
(e)
(f)
(g)
(h)
5 μm
10 μm

Figure 7

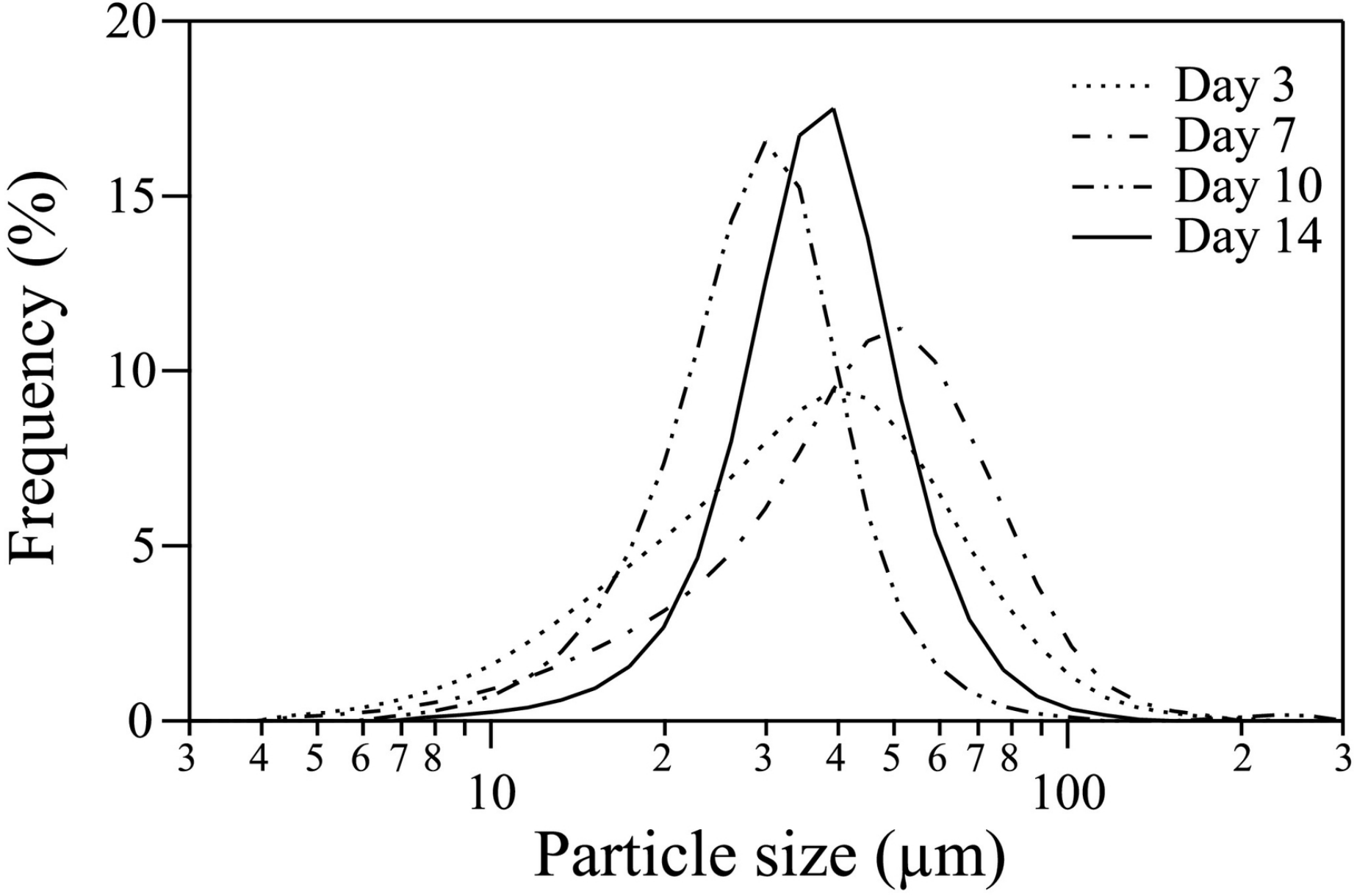
Day 3
Day 7
Day 10
Day 14
Frequency (%)
0
5
10
15
20
3 4 5 6 7 8
10
2 3 4 5 6 7 8
100
2 3
Particle size (μm)

Figure 8

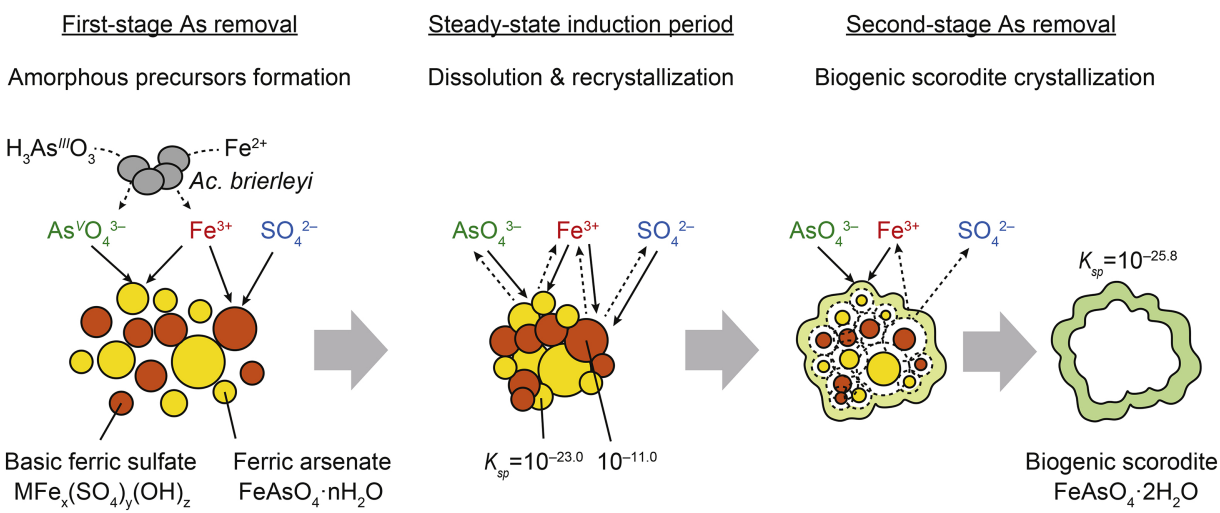
First-stage As removal
Amorphous precursors formation
Steady-state induction period
Dissolution & recrystallization
Second-stage As removal
Biogenic scorodite crystallization
$H_3As^{III}O_3$
Fe^{2+}
Ac. brierleyi
$As^{V}O_4^{3-}$
Fe^{3+}
SO_4^{2-}
AsO_4^{3-}
Fe^{3+}
SO_4^{2-}
AsO_4^{3-}
Fe^{3+}
SO_4^{2-}
K_{sp}=10$^{-25.8}$
K_{sp}=10$^{-23.0}$
10$^{-11.0}$
Basic ferric sulfate
$MFe_x(SO_4)_y(OH)_z$
Ferric arsenate
$FeAsO_4 \cdot nH_2O$
Biogenic scorodite
$FeAsO_4 \cdot 2H_2O$

Figure 9